

# Electrospraying Nanometer-Thin Elastomer Films for Low-Voltage Dielectric Actuators

Florian M. Weiss, Tino Töpfer, Bekim Osmani, Sven Peters, Gabor Kovacs, and Bert Müller\*

Micrometer-thin polymer films are often prepared using spin coating. In applications such as low-voltage dielectric elastomer actuators (DEAs), however, nanometer-thin polymer layers are required. In this paper, it is demonstrated that alternating current electro-spray deposition allows for the fabrication of high-quality nanometer-thin polydimethylsiloxane (PDMS) films. The growth of the PDMS with an average molecular weight of  $6000 \text{ g mol}^{-1}$  at rates of  $0.02\text{--}5.54 \text{ nm s}^{-1}$  was in situ monitored by means of spectroscopic ellipsometry. The Cauchy layer model performs above a deposition-rate-dependent average film thickness, which is associated with a confluent film. The droplet size measurements as the function of deposition rate show that inertia and polarization forces dominate in liquid PDMS electro-spraying. The roughness of the deposited films increases with the spray rate. After UV-light curing under Ar atmosphere, however, the films smoothen to root-mean-square roughness values between 0.20 and 0.28 nm determined by atomic force microscopy on areas of  $5 \mu\text{m} \times 5 \mu\text{m}$  and between 2 and 20 nm determined by interferometry on an area of  $0.72 \text{ mm}^2$ . Such electro-sprayed PDMS films with (sub-)nanometer roughness qualify for the fabrication of low-voltage DEAs.

## 1. Introduction

Dielectric elastomer actuators (DEAs) are relevant for a wide variety of applications including robotics,<sup>[1,2]</sup> haptics,<sup>[3]</sup> sound generation,<sup>[4]</sup> and lens systems<sup>[5,6]</sup> as well as in research of medical implants or artificial muscles.<sup>[7]</sup> The actual design depends on the specific application.<sup>[4,8,9]</sup> Most frequently, multistack DEAs<sup>[10,11]</sup> are fabricated to take advantage of reduced operating voltages. Nevertheless, the DEA microstructures require voltages of several hundred volts or above. For medical and other applications, however, the operating voltages have to be further

F. M. Weiss, T. Töpfer, B. Osmani, Prof. B. Müller  
Biomaterials Science Center  
University of Basel  
4123 Allschwil, Switzerland  
E-mail: bert.mueller@unibas.ch

F. M. Weiss, Dr. G. Kovacs  
Federal Laboratories for  
Materials Science and Technology  
8600 Dübendorf, Switzerland  
S. Peters  
SENTECH Instruments GmbH  
12489 Berlin, Germany

DOI: 10.1002/aelm.201500476



reduced, but strain values of the order of 10% should be achieved. Therefore, suitable techniques to prepare nanometer-thin, multistack DEAs consisting of silicone or other relevant polymers have to be developed. Spin-coated elastomer films that were reported to be thinner than that of casting, blading, and roll-to-sheet procedures are usually not thinner than  $5 \mu\text{m}$ .<sup>[11]</sup> Because of the limited adhesion forces between the elastomer and the underlying microstructure, spin coating only allows manufacturing multistack DEAs with a restricted number of layers on a finite area.

Electrospraying comprises a group of methods to build parts of products, which include ceramics,<sup>[12]</sup> carbon nanotubes,<sup>[13]</sup> polymers,<sup>[14–16]</sup> and composite materials.<sup>[17]</sup> Whereas the direct current mode is well established,<sup>[18–21]</sup> the alternate mode is still in the phase of development, as some recent studies on morphology

control<sup>[22]</sup> and frequency behavior<sup>[23–25]</sup> illustrate. We hypothesize that alternate current electro-spraying is also appropriate to prepare smooth submicrometer-thin polydimethylsiloxane (PDMS) films for DEAs.

We expect that ellipsometry allows for the in situ characterization of the growing PDMS film as previously carried out for direct current electro-spraying.<sup>[26]</sup> In situ ellipsometry not only enables the film thickness measurement<sup>[27–29]</sup> but also the phenomenological evaluation of the film surface roughness during deposition.<sup>[30–32]</sup> As the currently available models to be applied to the experimental ellipsometry data rely on serious assumptions, the extracted quantities must be validated with other methods after the termination of the deposition experiment.

In this paper, we not only deal with the deposition via alternate current electro-spraying but also with the subsequent curing by means of UV radiation. We presume to gain PDMS films with a root-mean-square roughness well below 1 nm.

## 2. Characterizing Electro-sprayed PDMS Films by Means of Ellipsometry

Figure 1A shows the experimental setup to monitor the electro-spray deposition by means of spectroscopic ellipsometry in situ. The data analysis was restricted to a spectral range of

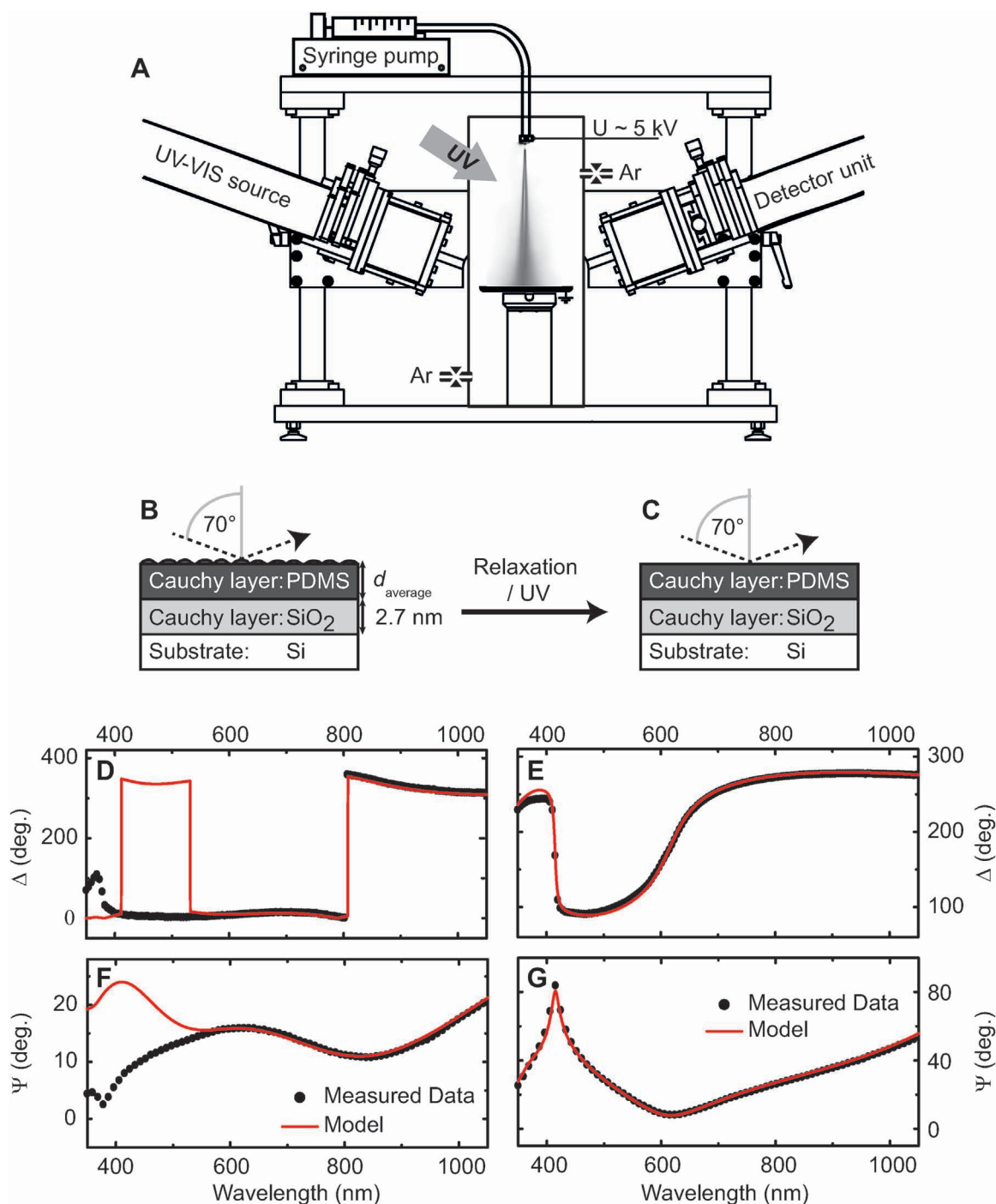


**Figure 1.** Electro spraying and in situ thin-film characterization using ellipsometry. A) Applying an alternating current, the electric field between nozzle and silicon substrate creates a spray of micrometer-size PDMS/solvent droplets traveling toward the substrate. The spectroscopic ellipsometer monitors the deposition and the subsequent UV curing under 1 bar Ar atmosphere. The schemes labeled B) and C) show the as-sprayed and the cured state of deposited thin films. Whereas the model according to these schemes only partly describes the  $\Psi$ - and  $\Delta$ -wavelength dependencies for the PDMS deposited with a mean rate of  $0.02 \text{ nm s}^{-1}$  (cf. diagrams (D) and (F)), the data recorded after curing can be perfectly fitted (cf. diagrams (E) and (G)). The PDMS film thickness, the lateral thickness gradient due to the spray profile and the extinction coefficient  $k_0$  for the deposited film and the UV-cured film result in  $(387 \pm 2) \text{ nm}$ ,  $(24 \pm 2) \text{ nm per mm}$ ,  $0.072 \pm 0.006$ , and  $(316.0 \pm 0.3) \text{ nm}$ ,  $(8 \pm 1) \text{ nm per mm}$ , and  $0.005 \pm 0.001$ , respectively.

300 to 1050 nm, as the absorption of PDMS is increasingly pronounced for wavelengths lower than 300 nm.<sup>[33]</sup> As baseline, we collected the ellipsometry data of the bare Si(100) substrate with its 2 to 3 nm thin, native oxide layer. We considered both

the native oxide and the sprayed PDMS as Cauchy layers (cf. Figure 1B,C) to extract the optical properties and the thickness of the growing film. The recorded  $\Psi$ - and  $\Delta$ -data depicted in Figure 1D–G correlate with the complex Fresnel reflection

coefficients  $r_p$  and  $r_s$  of p- and s-polarized light and their ratio  $\rho$ , described by the Fresnel equation

$$\rho = r_p/r_s = \tan \Psi \times e^{i\Delta} \quad (1)$$

The wavelength-dependent dielectric function  $\tilde{n}(\lambda)$  is extracted applying

$$\begin{aligned} \langle \tilde{n} \rangle^2 &= (\langle n \rangle + i \langle k \rangle)^2 \\ &= \sin(\varphi_0)^2 \times \left( 1 + \tan(\varphi_0)^2 \left( \frac{1-\rho}{1+\rho} \right)^2 \right) \end{aligned} \quad (2)$$

with  $\varphi_0$  representing the angle of the incident beam,  $n(\lambda)$  the real and  $k(\lambda)$  the complex parts of the refractive index. One of the simplest approximations according to the Cauchy series is the usage of a wavelength-independent, constant extinction coefficient

$$k(\lambda) = k_0 \quad (3)$$

and to reduce the wavelength dependence of the refractive index to

$$n(\lambda) = n_0 + c_1 n_1 / \lambda^2 \quad (4)$$

with  $c_1 = 100 \text{ nm}^2$ . This model is appropriate for the PDMS film in the wavelength range considered, as found in the present study. The agreement between the model and the experimental  $\Psi$ - and  $\Delta$ -data is quantified using the mean square error (MSE)

$$\frac{1}{N} \sqrt{\sum_{i=1}^N \left\{ \left( \frac{\Psi_i^m - \Psi_i^{\text{th}}}{\delta \Psi} \right)^2 + \left( \frac{\Delta_i^m - \Delta_i^{\text{th}}}{\delta \Psi} \right)^2 \right\}} \quad (5)$$

During the initial stages of growth, however, neither the fitting according to the Cauchy layer model nor the fitted data by the effective medium layer model<sup>[34]</sup> were reasonable, presumably because of the droplets present on the substrate. At advanced stages of growth, the fitting according to the Cauchy layer model becomes possible as displayed in the diagrams of Figure 1D,F. Here, we assume that the droplets start to form a confluent layer with a rough morphology reflected in the fitted constant extinction coefficient  $k_0$ . Here,  $k_0$  simulates the scattering of light at the protrusions on the growing surface. In this context, however,  $k_0$  is rather a phenomenological parameter to describe the damping of the  $\Psi$ - and  $\Delta$ -amplitudes by light scattering at rough surfaces. Thus, the wavelength dependency of  $k$  was neglected.

In order to corroborate the applicability of the fitting procedure described above, we have characterized the films after the termination of the deposition and the curing using UV radiation. The diagrams of Figure 1E,G clearly point the much better fitting according to the Cauchy layer model.

The optical properties of the deposit DMS-V21 resulted from ellipsometry measurements on a 2  $\mu\text{m}$  thick film spin-coated with a smooth morphology. The root-mean-square roughness value corresponds to  $(0.85 \pm 0.01) \text{ nm}$ . The Cauchy coefficients

were determined to  $n_0 = 1.396 \pm 0.005$  and  $n_1 = 37 \pm 1$ , and  $k_0 = 0$ .

Using this approximation, the fitting of the data represented in Figure 1D–G gives rise to a film thickness of  $(387 \pm 2) \text{ nm}$ . The lateral thickness gradients as the result of the spray profile are not considered.

The combined fits of the experimental data given in the diagrams of Figure 1D,F using a constant extinction coefficient results in a  $k_0$ -value of  $0.19 \pm 0.06$ . It indicates a rough surface. One detects major discrepancies between model and experimental data below 600 nm, which leads to the MSE of 53. After UV light curing, the extinction coefficient  $k_0$  equals to  $0.010 \pm 0.002$  and the MSE to 3.5 (see fit in the diagrams of Figure 1E,G). This experimentally observed reduction of light scattering is interpreted as surface smoothing through reordering and relaxation of the polymer chains mediated by the UV light.

### 3. Ellipsometry Measurements During Electro spraying

Above, we demonstrated that the Cauchy model is sufficient to extract the film thickness after the termination of film growth. During the initial stages of film growth, however, the determination of the average PDMS thickness is complex, since the individual droplets form islands and lead to a rough surface morphology. Nevertheless, the  $\Psi$ - and  $\Delta$ -data are acquired even during the early stages of electro spray deposition. The diagram in Figure 2A displays the  $\Psi$ - and  $\Delta$ -data obtained at a wavelength of 632 nm for the selected flow rate of 267 nL s<sup>-1</sup>. The angles  $\Psi$  and  $\Delta$  start from 160° and 10°, before they oscillate with decreasing amplitudes between 80° and 90° and between 27° and 37°, respectively. Table S1 (Supporting Information) lists the data to show the temporal evolution in detail. The observed oscillations are the consequence of interferences at the selected wavelength. After the termination of deposition, the film thickness was determined to  $(1420 \pm 1) \text{ nm}$  taking advantage of the Cauchy coefficients derived above. It is reasonable to assume a constant growth rate over the spray period of 1250 s. This knowledge is applied to derive both the refractive index and the extinction coefficient as the function of the average film thickness (see Figure 2B). For average film thicknesses below 300 nm, the fit does not converge and the related data cannot be obtained. Above that threshold, the fit converges, and the two optical parameters are derived. The refractive index  $n(\lambda = 632 \text{ nm})$  starts above 1.13, a superposition of PDMS/solvent droplets and air, and asymptotically reaches the bulk value of PDMS, which corresponds to 1.396 in agreement with published data.<sup>[35]</sup> Similarly, the extinction coefficient  $k_0$  exponentially converges to  $0.08 \pm 0.02$ . The surface roughness decreasing as the deposition proceeds explains this asymptotical behavior of the two optical constants.

A constant refractive index simplifies the determination of the film thickness on the basis of the ellipsometry data. One may, therefore, consider regimes, where the refractive index deviates from the bulk value by less than 5%, i.e., it is within the interval  $1.325 < n < 1.396$ , suitable for such an approximation. As shown by the gray-shaded area in Figure 2B, such an

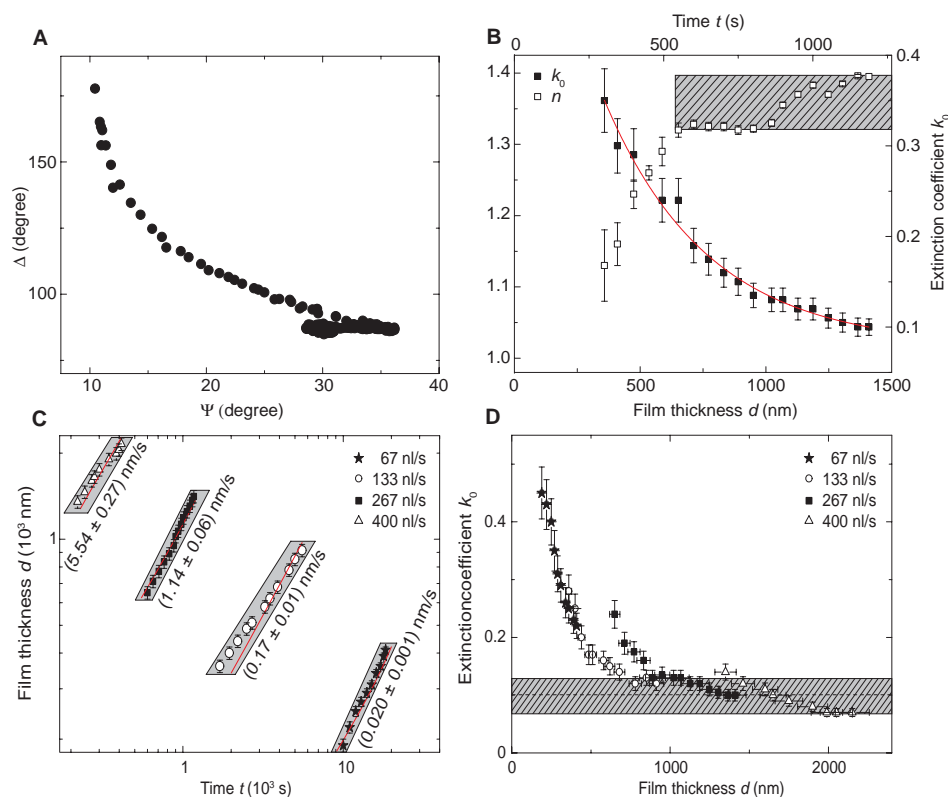


**Figure 2.** Ellipsometry measurements during electrospaying. A)  $\Psi$ - and  $\Delta$ -values were ellipsometrically measured using a wavelength of 632 nm during the PDMS/solvent deposition with a flow rate of 267 nL s<sup>-1</sup>. The damped oscillatory behavior comes from interferences of the monochromatic light with the surface structures corresponding in size to the applied wavelength. Table S1 (Supporting Information) lists the data to present the time lapse. B) At the deposition rate of 1.2 nm s<sup>-1</sup>, the refractive index  $n$  and the extinction coefficient  $k_0$  cannot be reasonably fitted for films thinner than 300 nm. For larger film thicknesses, the values asymptotically approach their limits. For films thicker than 520 nm, one may assume a constant refractive index (cf. gray-shaded area). C) The measurement of the PDMS film thickness for the flow rates 67, 133, 267, and 400 nL s<sup>-1</sup> allows for the determination of the growth rates from the slopes, which correspond to (0.020 ± 0.001), (0.17 ± 0.01), (1.14 ± 0.06), (5.54 ± 0.27) nm s<sup>-1</sup>, respectively. There is a flow-rate-dependent critical thickness below which no reasonable fit of the ellipsometry data is obtained. D) The extinction coefficient  $k_0$  reduces as the growth proceeds. For films thicker than 1000 nm, the extinction coefficient  $k_0$  stays within a well-defined range indicated by the gray-shaded area and may be regarded as constant.

approximation is reasonable for film thicknesses above 650 nm and deposition times exceeding 550 s. For these regimes, however, the experimentally derived extinction coefficient  $k_0$  shows a significant decrease associated with the light scattering at the rough surface. Nevertheless, for the in situ monitoring of electrospayed films, a critical thickness should be selected to work with a constant refractive index of the Cauchy layer.

The validity of this approach can be checked measuring the film thickness as the function of the deposition time. Providing a constant deposition rate, a linear dependence is expected. Figure 2C validates this behavior for the selected flow rates of 67, 133, 267, and 400 nL s<sup>-1</sup>. The slopes of the related fits (see red-colored full lines) lead to the growth rates of PDMS and correspond to 0.02, 0.17, 1.2, and 5.5 nm s<sup>-1</sup>, respectively. It should be noted that the film thicknesses at growth termination are in agreement with the results of 3D laser microscopy.

The films are sprayed in the multicone jet mode (cf. photographs of Figure S1, Supporting Information).<sup>[36]</sup> Thus, the deposition rate locally varies. This variation is not necessarily fully taken into account in the ellipsometric measurements and the related error bars of the derived film thicknesses.

For this reason, the estimations are included into the diagram of Figure 2C using the gray-shaded areas.

Figure 2C allows reading the critical thicknesses for the selected deposition rates. This thickness increases from 170 via 360 and 520 to 1030 nm for the four selected rates between 67 and 400 nL s<sup>-1</sup>. This behavior presumably reflects the flow-rate-dependent droplet size. According to scaling laws with dominating inertia and polarization forces valid for ethyl acetate,<sup>[37]</sup> the droplet diameter  $D$  depends on the square root of the flow rate  $Q$ . Admixing 5 vol% of PDMS to ethyl acetate obviously does not remarkably change the physical properties responsible for the electrospay process. This behavior is in line with the data represented in Figure 2D. At a certain film thickness, the extinction coefficient was found to be higher with increasing flow rate. Nonetheless, for films thicker than 1000 nm and the flow rates investigated, the extinction coefficient stays within the range indicated by the gray-shaded area. To simplify matters, it may be regarded as constant. For these thicknesses, the influence of a droplet surface is smaller compared to the compact part of the PDMS film.

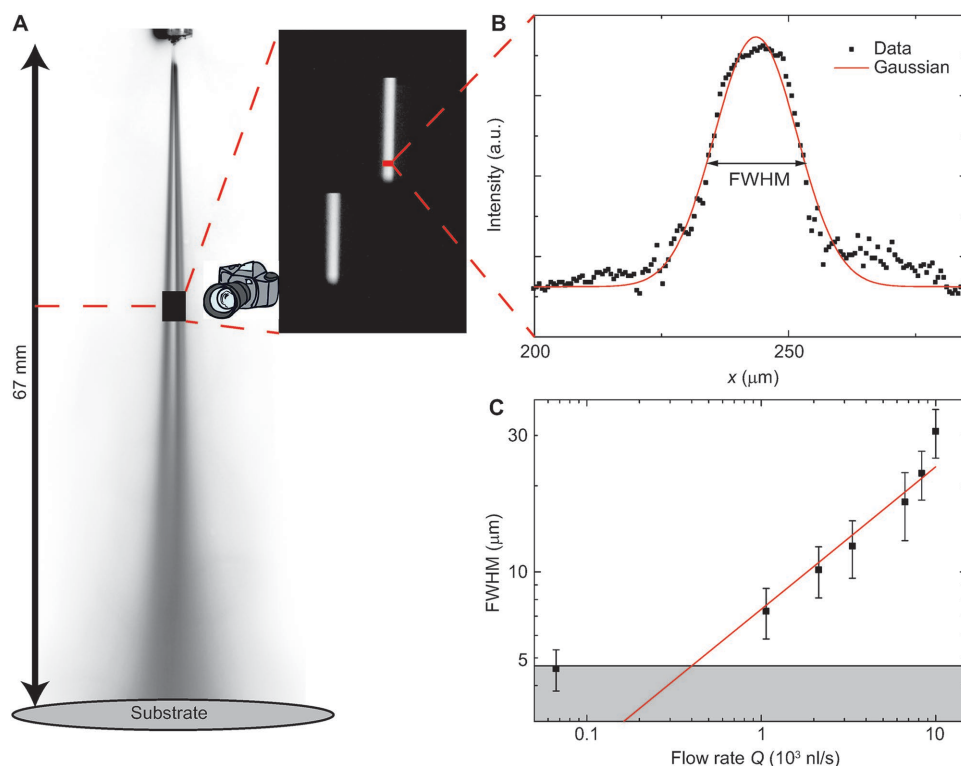


**Figure 3.** Flow-rate-dependent droplet size. A) Scheme of the experimental setup to determine the droplet diameter as the function of the flow rate. The photograph shows the path of two droplets during the 125  $\mu\text{s}$  exposure time. B) The droplet diameter can be characterized by the FWHM values derived from a Gaussian fit. C) The FWHM depends on the square root of the flow rate. The experimental setup does not permit reliably measuring FWHM values below 5  $\mu\text{m}$  because of the limited spatial resolution.

#### 4. Determination of the Drop Sizes in the Jet

The ellipsometric results are corroborated using optical images of the droplets and looking for the scaling law proposed by Gañán-Calvo.<sup>[37]</sup> The exemplary photograph of the droplet's trajectory in **Figure 3A** gives rise to a cross-section that follows a Gaussian distribution (cf. **Figure 3B**). Integrating the data along the droplet path and fitting them, one can easily access the full-width at half-maximum (FWHM). **Figure 3C** shows a double-logarithmic plot of FWHM values derived from at least six trajectories per flow rate as the function of the flow rate. The slope exactly corresponds to the predicted behavior with the exception of the value for 67  $\text{nL s}^{-1}$ . The exception is explained by the limited spatial resolution of the experimental setup. Data located in the gray-shaded area are therefore overestimated.

#### 5. UV Curing of Electrospayed PDMS Films

The spectroscopic ellipsometer was also applied in situ study the alteration of the PDMS film during curing. During this treatment, the extinction coefficient is obviously decreasing. After a treatment period of 1000 s, the extinction coefficient  $k_0$  reaches values between 0.04 and 0.08 for the applied flow rates (see **Figure 4A**). It should be mentioned that this phenomenon could also be represented by a lateral gradient converging  $k_0$  to zero. The decrease of the extinction coefficient can be understood as surface smoothing. Optical interferometry studies

on an area of 982  $\mu\text{m} \times 739 \mu\text{m}$ , i.e., about six times smaller than the spot size of the ellipsometer, support this description. The root-mean-square roughness values, measured after the curing, correspond to  $(15.1 \pm 3.1) \text{ nm}$ . The variation of the roughness values is therefore well comparable with the variation of the extinction coefficient.

The as-sprayed film flattens due to its well-known viscoelastic behavior, which is particularly valid for the PDMS with the relatively smaller molecular weight of 6000  $\text{g mol}^{-1}$ . The use of UV light accelerates the flattening. Therefore, it is stated that the UV light mediates the smoothing of the electrospayed thin films.

Surprisingly, the surface roughness after curing is independent on the applied flow for deposition rates between 0.02 and 5.5  $\text{nm s}^{-1}$ . In order to verify this experimental result, we investigated the surface morphology by means of atomic force microscopy (AFM). The images with a size of 5  $\mu\text{m} \times 5 \mu\text{m}$  displayed in **Figure 4B–E** support our conclusion and provide a homogeneous film with a root-mean-square roughness between 0.20 and 0.28  $\text{nm}$ .

Preliminary data concerning the deposition of PDMS with larger molecular weights show a similar behavior but as expected a rougher surface morphology.

The atomic force microscope used in the present study allows not only measuring the morphology but also determining the mechanical properties of the PDMS films. The electrospayed films exhibit an elastic modulus of  $(1.5 \pm 0.3) \text{ MPa}$  after curing. The elastic modulus of the spin-coated film

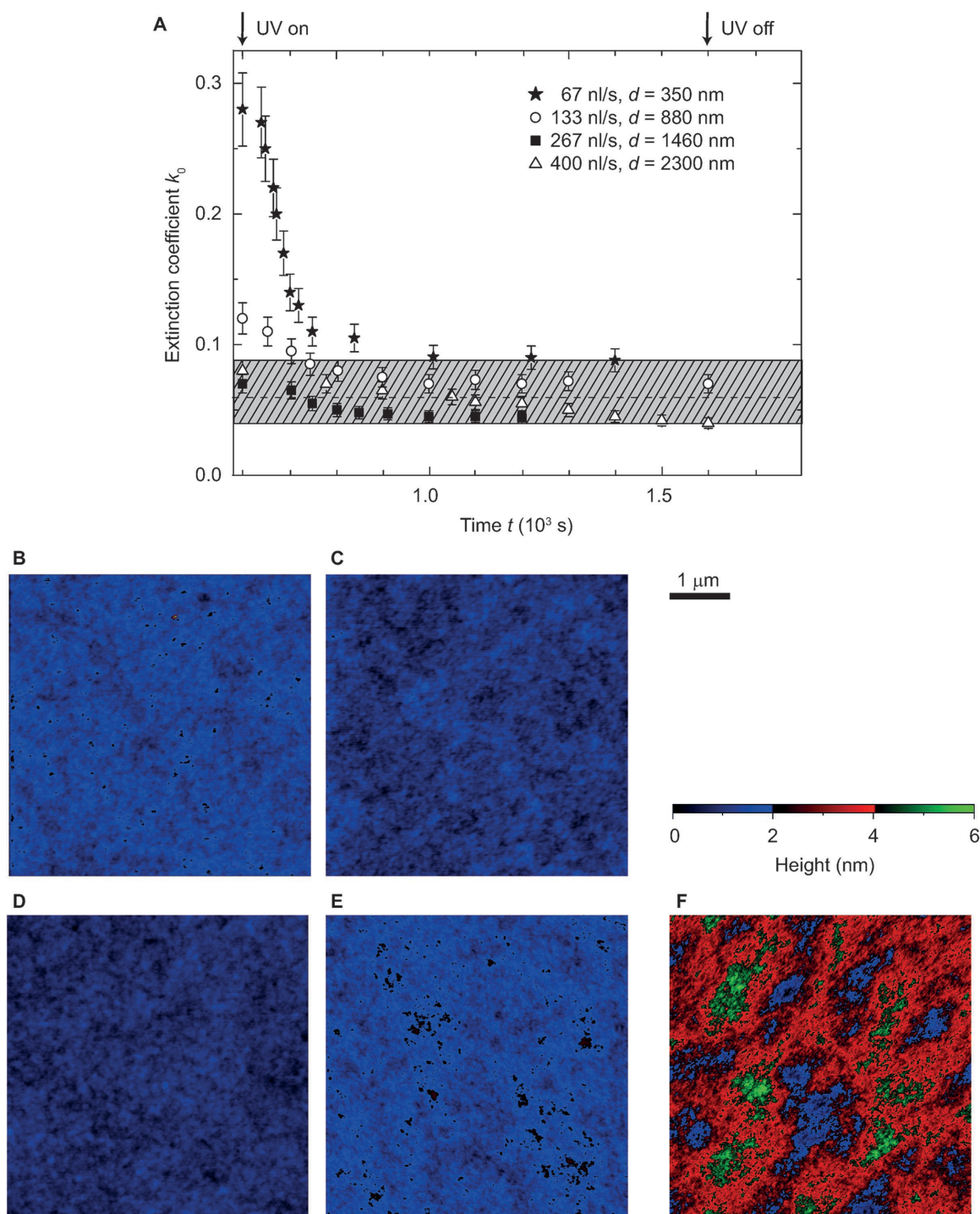


**Figure 4.** Deposition-rate-independent surface roughness after UV curing. A) During UV irradiation the extinction coefficient of the PDMS thin film becomes smaller. It approaches values between 0.04 and 0.08 for the deposition rates applied for thin-film formation, as shown by the gray-shaded area. B–E) The AFM images compare the surface morphology of UV-light-cured PDMS films for flow rates between 67 and 400  $\text{nL s}^{-1}$  with an average film thickness of 340 nm. As one cannot identify significant differences between the images and their root-mean-square roughness values, the results support the statement that the final surface morphology is independent of the deposition rate. F) The AFM image of the 2  $\mu\text{m}$  thick spin-coated PDMS film exhibits about three times larger roughness than the electrospayed thin films. The color bar for the height information and the 1  $\mu\text{m}$  length bar apply for the five AFM images presented.

corresponds to  $(4.7 \pm 0.3)$  MPa after curing. Hence, one can conclude that the electrospayed films are stable enough for actuator applications.

Since the present study restricts to the PDMS film preparation and characterization, the electronic application in a DEA system will be presented in a forthcoming communication.

## 6. Conclusion

Alternating current electrospray deposition of micrometer-size ethyl acetate droplets containing 5% vinyl-terminated PDMS allows preparing PDMS films with deposition rates as currently used in micro- and optoelectronics but with a root-mean-square roughness for the surface three times smaller than advanced spin-coating applying rotation speeds as high as 5000 revolutions per minute. Whereas spin coating results in PDMS films that are very few micrometers thick or slightly below one micrometer, the electrospraying enables us to fabricate PDMS films well below one micrometer with smaller roughness. As the operation voltage of a DEA—to reach a constant strain—quadratically follows the elastomer thickness, this moderate improvement is an essential step toward low-voltage DEA with reasonable breakdown voltage.

## 7. Experimental Section

**Materials and Setup:** In a first step, the liquid vinyl-terminated PDMS polymers (DMS-V21,  $M_w$  6 kDa, Gelest, USA) were dissolved in ethyl acetate (Laboratory reagent grade, Fisher Scientific UK, Brunschwig, Basel, Switzerland) to obtain a 5 vol% concentration. This solution was stirred for 1 h and left for 3 d to make sure that the chains are no longer entangled. Chemicals were used as purchased without any further purification. The polymer solution was then drawn up into a 2 mL glass syringe with metallic Leur-lock (Eternal-Matic, Sanitex, HUBERLAB, Aesch, Switzerland) and connected to a metallic nozzle (26 s, Hamilton, Bonaduz, Switzerland) with an inner diameter of 0.13 mm. The syringe itself was mounted on a syringe pump (Aladdin six syringe pump, World Precision Instruments Germany GmbH, Berlin, Germany) to vary the flow rate between 0.13 and 660 000 nL s<sup>-1</sup>. The nozzle is connected to the voltage source (TREK, 5/80, Lockport, NY, USA) and coupled with the function generator (Model 119M, Max Meier Elektronik, Zurich, Switzerland) in order to apply a rectangular voltage function of  $\pm 5$  kV with a frequency of 18 Hz, which was monitored by an Tektronix oscilloscope (TDS 210, Computer Control AG, Zurich, Switzerland) throughout all experiments of this study. The distance from the nozzle to the Si substrate (SiMat, Silicon Materials, Kaufering, Germany) was kept constant to 67 mm. For cleaning purposes, the Si wafers were rinsed with acetone (Merck KGaA, Darmstadt, Germany) and ethyl acetate. The UV cure was accomplished in Ar (Messer Schweiz AG, Lenzburg, Switzerland) atmosphere of 1 bar applying radiation of a deuterium broad-band UV lamp (Yuyu Lightning, China) covering a spectral range between 180 and 450 nm with its maximum intensity at a wavelength of 210 nm with a distance of 2 cm.

**Real-Time Spectroscopic Ellipsometry:** Ellipsometry was used to monitor the film growth, its relaxation, and the UV light curing process. Utilizing the spectroscopic ellipsometer SE801 from SENTECH (Berlin, Germany), controlled by the SpectraRay3 software, either  $\Psi$  and  $\Delta$  or the Fourier coefficients  $S_1$  and  $S_2$  were determined as a function of the wavelength between 300 and 1050 nm. The incident beam angle, 70° from the normal, with a beam diameter of 2 mm gave rise to a spot size of 2 mm  $\times$  5 mm on the wafer's surface. The in situ measurement period was set to 1 s steps. The linear and first order nonlinear refractive indices of the DMS-V21 were determined by a static measurement of a spin-coated, 2  $\mu$ m thick film and had values of  $n_0 = 1.396 \pm 0.005$  and  $n_1 = 37 \pm 0.7$ , respectively. The wavelength-independent extinction coefficient  $k_0$  was utilized to simulate the scattering at the surface.

**Spin-Coating:** For a reference of the optical properties of PDMS, a sample of DMS-V21 was spin-coated (WS-400B-6NPP/LITE/AS, Laurell Technologies Corporation, North Wales, PA, USA) on a Si wafer with 5000 rpm for a period of 150 s to obtain a 2  $\mu$ m thick film, which was subsequently measured by ellipsometry as described above.

**3D Laser Scanning Microscopy:** By cutting the cured PDMS layer, a step edge was generated to obtain the layer thickness with optical profilometry by means of a 3D laser scanning microscopy (Keyence VK-X200, Keyence International, Belgium).<sup>[38]</sup>

**Image SXM 139:** Evaluation of the drop size was done by taking pictures (Canon 60D) of the spray with an exposure time of 125  $\mu$ s with a magnification of 2.5 (Stermi DV4 SPOT, Carl Zeiss AG, Feldbach, Switzerland). Using Image SXM, the diameter was determined integrating over the width from single cross-sections of the traces obtained in the photograph and taking their mean value. The error was estimated by the FWHM values of the integrated trace widths distribution.

**Atomic Force Microscopy:** AFM measurements ( $5 \times 5 \mu\text{m}^2$ , tapping mode, vibration amplitude 500 mV, set point 20%) were performed using a FlexAFM System (Nanosurf AG, Liestal, Switzerland). 2048 lines at a speed of 768 ms were acquired for each image using a noncontact soft tapping AFM probe (PPP-NCSTR probe, tip radius < 7.0 nm, NanoAndMore GmbH, Wetzlar, Germany). The raw data were leveled removing a polynomial background of the second degree and fixing the color range from zero to 2 nm. Root-mean-square values were calculated using the Gwyddion 2.41 software (Gwyddion: an open-source software for scanning probe microscopy (SPM) data analysis, <http://gwyddion.net>).

The mechanical properties of the spin-coated and electrosprayed films were assessed by atomic force microscopy (FlexAFM C3000, Nanosurf AG, Switzerland). To this end, 100 indentations on 90  $\mu$ m  $\times$  90  $\mu$ m arrays were acquired with a spherical tip with a radius of 150 nm (B150\_FMR, Nanotools GmbH, Germany) at a load of 50 nN. The mean elastic moduli of the cured PDMS films were calculated using the FLEX-ANA (Automated Nanomechanical Analysis) software from Nanosurf. Potential substrate effects can be neglected since the indentation depths were well below 100 nm.

**Interferometry:** In order to obtain the surface morphology of the UV light-cured films in a spot size of 982  $\mu$ m  $\times$  739  $\mu$ m, a 3D Optical Surface Metrology System (DCM8, Leica Microsystems AG, Heerbrugg, Switzerland) with a Leica Interferential Mirau SR 50 $\times$  objective was used. The number of points in x- and y-directions was 3808 and 2866 with 258 nm spacing.

## Supporting Information

Supporting Information is available from the Wiley Online Library or from the author.

## Acknowledgements

The financial support of the Swiss National Science Foundation (project 200021-135496) and the nano-tera.ch initiative (project SmartSphincter) as well as the Swiss Nanoscience Institute (SNI) for the financial contribution to the AFM is gratefully acknowledged. The authors thank Thomas Geiger for supporting the interferometric measurements at the Federal Laboratories for Materials Science and Technology (Empa) and Monica Schönenberger from the Nanotech Service Lab for assistance at the 3D Laser microscope.

Received: December 23, 2015

Revised: January 19, 2016

Published online:

- [1] Y. Bar-Cohen, *Proc. SPIE* **2002**, 4695, 1.
- [2] Q. Pei, R. Pelrine, S. Stanford, R. Kornbluh, M. Rosenthal, *Synth. Met.* **2003**, 135, 129.
- [3] M. Y. Ozsecen, M. Sivak, C. Mavroidis, *Proc. SPIE* **2010**, 7647, 764737.

- [4] R. Heydt, R. Kornbluh, J. Eckerle, R. Pelrine, *Dielectric Elastomers as Electromechanical Transducers: Fundamentals, Materials, Devices, Models and Applications of an Emerging Electroactive Polymer Technology*, Elsevier Science, Oxford **2008**.
- [5] F. Carpi, G. Frediani, S. Turco, D. De Rossi, *Adv. Funct. Mater.* **2011**, 21, 4152.
- [6] S. Shian, R. M. Diebold, D. R. Clarke, *Opt. Express* **2013**, 21, 8669.
- [7] B. Müller, H. Deyhle, S. Mushkolaj, M. Wieland, *Swiss Med. Wkly.* **2009**, 139, 591.
- [8] G. Kofod, M. Paajanen, S. Bauer, *Proc. SPIE* **2006**, 6168, 61682J.
- [9] P. Lochmatter, *Ph.D. Thesis*, ETH Zürich, Zürich **2006**, 330.
- [10] F. Carpi, C. Salaris, D. De Rossi, *Smart Mater. Struct.* **2007**, 16, S300.
- [11] P. Lotz, M. Matysek, H. F. Schlaak, *IEEE/ASME Trans. Mechatronics* **2011**, 16, 58.
- [12] A. Jaworek, *J. Mater. Sci.* **2007**, 42, 266.
- [13] J. N. O'Shea, J. B. Taylor, J. C. Swarbrick, G. Magnano, L. C. Mayor, K. Schulte, *Nanotechnology* **2007**, 18, 035707.
- [14] K. Altmann, R. D. Schulze, G. Hidde, J. Friedrich, *J. Adhes. Sci. Technol.* **2012**, 27, 988.
- [15] K. Morota, H. Matsumoto, T. Mizukoshi, Y. Konosu, M. Minagawa, A. Tanioka, Y. Yamagata, K. Inoue, *J. Colloid Interface Sci.* **2004**, 279, 484.
- [16] I. B. Rietveld, K. Kobayashi, H. Yamada, K. Matsushige, *J. Colloid Interface Sci.* **2006**, 298, 639.
- [17] Y. S. Kim, *Sens. Actuators B* **2010**, 147, 137.
- [18] A. C. Sullivan, S. N. Jayasinghe, *Biomicrofluidics* **2007**, 1, 034103.
- [19] J. Ju, Y. Yamagata, T. Higuchi, *Adv. Mater.* **2009**, 21, 4343.
- [20] G. Xin, H. Sun, T. Hu, H. R. Fard, X. Sun, N. Koratkar, T. Borca-Tasciuc, J. Lian, *Adv. Mater.* **2014**, 26, 4521.
- [21] S. M. Mirvakili, J. E. Slota, A. R. Usgaocar, A. Mahmoudzadeh, D. Jun, M. N. Mirvakili, J. T. Beatty, J. D. W. Madden, *Adv. Funct. Mater.* **2014**, 24, 4789.
- [22] L. Y. Yeo, Z. Gagnon, H.-C. Chang, *Biomaterials* **2005**, 26, 6122.
- [23] R. Kessick, J. Fenn, G. Tepper, *Polymer* **2004**, 45, 2981.
- [24] S. Maheshwari, H.-C. Chang, *Appl. Phys. Lett.* **2006**, 89, 234103.
- [25] L. Y. Yeo, D. Lastochkin, S.-C. Wang, H.-C. Chang, *Phys. Rev. Lett.* **2004**, 92, 133902.
- [26] T. Ino, T. Hiata, T. Fukuda, K. Ueno, H. Shirai, *J. Non-Cryst. Solids* **2012**, 358, 2520.
- [27] C. Cai, M. M. Bösch, B. Müller, Y. Tao, A. Kündig, C. Bosshard, Z. Gan, I. Biaggio, I. Liakatas, M. Jäger, *Adv. Mater.* **1999**, 11, 745.
- [28] B. Müller, M. Jäger, Y. Tao, A. Kündig, C. Chengzhi, C. Bosshard, P. Günter, *Opt. Mater.* **1999**, 12, 345.
- [29] R. P. Netterfield, P. J. Martin, W. G. Sainty, R. M. Duffy, C. G. Pacey, *Rev. Sci. Instrum.* **1985**, 56, 1995.
- [30] D. Lehmann, F. Seidel, D. Zahn, *SpringerPlus* **2014**, 3, 1.
- [31] T. A. Mykhaylyk, N. L. Dmitruk, S. D. Evans, I. W. Hamley, J. R. Henderson, *Surf. Interface Anal.* **2007**, 39, 575.
- [32] X. Ziang, L. Shifeng, Q. Laixiang, P. Shuping, W. Wei, Y. Yu, Y. Li, C. Zhijian, W. Shufeng, D. Honglin, Y. Minghui, G. G. Qin, *Opt. Mater. Express* **2014**, 5, 29.
- [33] J. Lee, J. Kim, H. Kim, Y. M. Bae, K.-H. Lee, H. J. Cho, *J. Microchem. Microeng.* **2013**, 23, 035007.
- [34] D. A. G. Bruggeman, *Ann. Phys.* **1935**, 416, 665.
- [35] B. Schnyder, T. Lippert, R. Kötz, A. Wokaun, V.-M. Graubner, O. Nuyken, *Surf. Sci.* **2003**, 532–535, 1067.
- [36] M. Cloupeau, B. Prunet-Foch, *J. Electrostat.* **1990**, 25, 165.
- [37] A. M. Ganan-Calvo, *J. Fluid Mech.* **2004**, 507, 203.
- [38] M. Conroy, J. Armstrong, *J. Phys.: Conf. Ser.* **2005**, 13, 458.